ACS Partner Journal

ACCOUNTS
—of materials research—

pubs.acs.org/amrcda

Article

Methodologies to Improve the Stability of High-Efficiency Perovskite Solar Cells

Sanjay Sandhu and Nam-Gyu Park*

Cite This: *Acc. Mater. Res.* 2024, 5, 1544−1557

Read Online

ACCESS | Metrics & More | Article Recommendations

CONSPECTUS: Organic−inorganic lead halide perovskite solar cells (PSCs) have attracted significant interest from the photovoltaic (PV) community due to suitable optoelectronic properties, low manufacturing cost, and tremendous PV performance with a certified power conversion efficiency (PCE) of up to 26.5%. However, long-term operational stability should be guaranteed for future commercialization. Over the past decade, intensive research has focused on improving the PV performance and device stability through the development of novel charge transport materials, additive engineering, compositional engineering, interfacial modifications, and the synthesis of perovskite single crystals. In this Account, we provide a comprehensive overview of recent progress and research directions in the fabrication of highly efficient and stable PSCs, including key outcomes from our group. We begin by highlighting the critical challenges and their causes that are detrimental to the development of stable PSCs. We then discuss the fundamentals of halide perovskites including their optical and structural properties. This is followed by a description of the fabrication methods for perovskite crystals, films, and various device architectures. Next, we introduced target-oriented key strategies such as developing high-quality single crystals for redissolution as a perovskite precursor to fabricate phase-stable and reproducible PSCs, along with reduced material costs, employing multifunctional additives to get uniform, robust, and stable perovskite films, and interfacial engineering techniques for effective surface and buried interface defect passivation to improve charge transport and long-term stability. Finally, we conclude with a critical assessment and perspective on the future development of PSCs. This Account will provide valuable insights into the current state-of-the-art PSCs and promising strategies tailored to specific roles that can be combined to manipulate the perovskite structure for novel outcomes and further advancements.

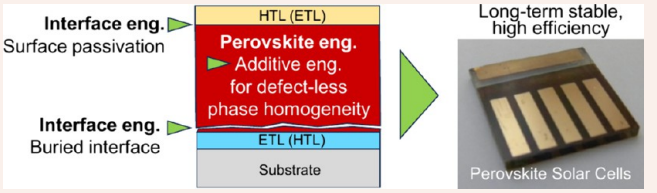

1. INTRODUCTION

Organic−inorganic hybrid lead halide perovskite (OIHP) materials are at the center of photovoltaic (PV) technology and have received huge research interest, because of their exceptional optoelectronic properties, such as tunable bandgap, high absorption coefficient (10^4−10^5 cm^{-1}), low exciton binding energy (10−50 meV), long carrier diffusion length (up to 1 mm), and high charge carrier density (>10^{17} cm^{-2}).[1] The power conversion efficiency (PCE) of perovskite solar cells (PSCs) has skyrocketed since the groundbreaking report in 2012, where a solid-state PSC with an appreciable PCE of 9.7% and stability up to 500 h was reported for the first time.[2] PSCs have demonstrated great potential to be considered as a next-generation promising PV technology, reaching a certified PCE of over 26% under one-sun illumination, which is on par with silicon and higher than those of cadmium telluride (CdTe) and copper−indium−gallium-arsenide (CIGS)-based solar cells.[3,4] This rapid PCE improvement over the past decade is accomplished by advancements in material chemistry and fabrication process engineering strategies.

However, despite achieving a commendable PCE, the stability of PSCs under extrinsic environmental factors (such as oxygen and moisture) and intrinsic operational conditions (such as light, electrical bias, and heat) remains far below the stability standards required for commercialization. The long-term stability under maximum power point tracking (MPPT), electrical bias, and other aggressive stress factors—including high relative humidity (RH), elevated temperatures (T = 65 or 85 °C), damp heat test (85% RH, along with elevated T), and light-dark cycling—needs significant improvement to meet the stability protocols set by the International Summit on Organic Photovoltaic Stability (ISOS).[5] A typical PSC architecture consists of multiple layers, including the perovskite active layer, charge transport layers (CTLs), and electrodes; where device stability is influenced by the properties of each individual layer under external stimuli. The degradation of PSCs is triggered by material instability, phase transitions and segregation, ion migration, charge carrier accumulation, weak interfaces, trap

Received: July 22, 2024
Revised: September 17, 2024
Accepted: October 12, 2024
Published: October 30, 2024

https://doi.org/10.1021/accountsmr.4c00237
Acc. Mater. Res. 2024, 5, 1544−1557

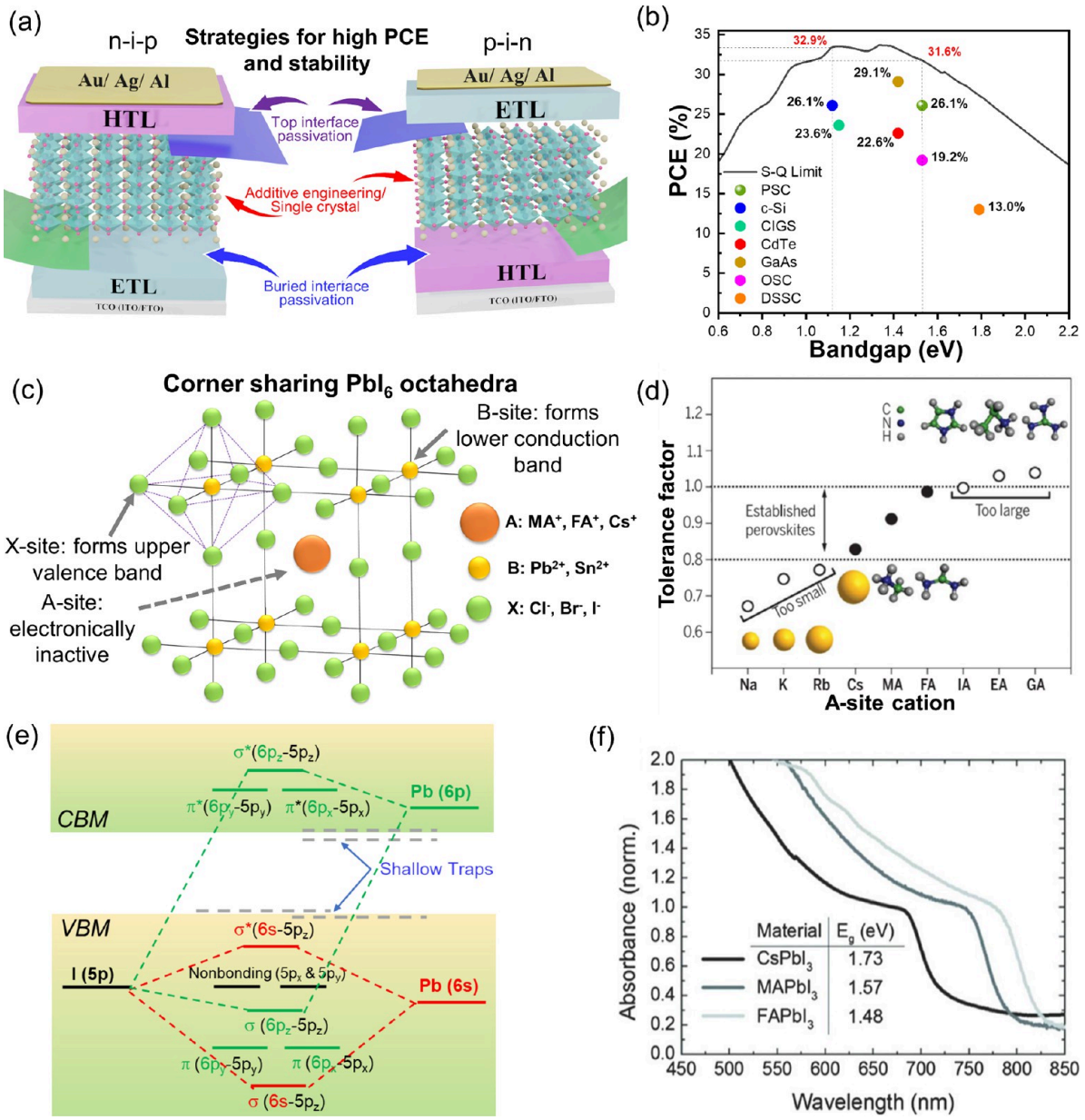

Figure 1. (a) Schematic of various engineering strategies employed to improve PV performance of PSCs, (b) SQ limit and maximum PCE obtained for various solar cells, and (c) schematic unit cell structure of ABX_3 perovskite. (d) TF of perovskite materials with different A-site cations. [Reproduced with permission from ref 12. Copyright 2017, AAAS.] (e) Electronic band structure of the $APbI_3$ perovskite. (f) UV−vis absorbance spectra of different perovskite materials. [Reproduced with permission from ref 14. Copyright 2014, Royal Society of Chemistry, London.]

states/defects at grain boundaries, detrimental changes in the properties of CTLs, and ion exchange at the interfaces during solar cell's operation and storage under ambient conditions.[6] Therefore, to further enhance PV performance and device stability, recent research efforts have been devoted to limiting these detrimental factors. This includes the development of interfacial materials for stable and robust passivation of both buried and top surfaces, compositional engineering for stable perovskite phases, additives to mitigate defect formation and enhance light-soaking stabilities, novel dopant-free hole transport materials (HTMs) or noncorrodible dopants, thermally stable *p-i-n* structures, and high-quality single crystal synthesis methods for low-cost and phase-stable perovskite materials (Figure 1a).[7−10]

In this Account, we offer an in-depth commentary on recent research directions, including groundbreaking reports from our group, aimed at enhancing PCE, stability, and a fundamental understanding of PSCs. We begin by discussing the structural properties of key perovskite materials and flagged major concerns related to their performance and phase variations. This is followed by a brief description of the fabrication methods for thin films and single crystals. We then summarize key strategies, along with their specific roles, and review recent research conducted in each direction specifically targeted on improving stability through single crystal engineering, additives, and interface passivation strategies. At the end, we provide an overall assessment and outline potential research strategies to further advance PSC technology.

https://doi.org/10.1021/accountsmr.4c00237
Acc. Mater. Res. 2024, 5, 1544−1557

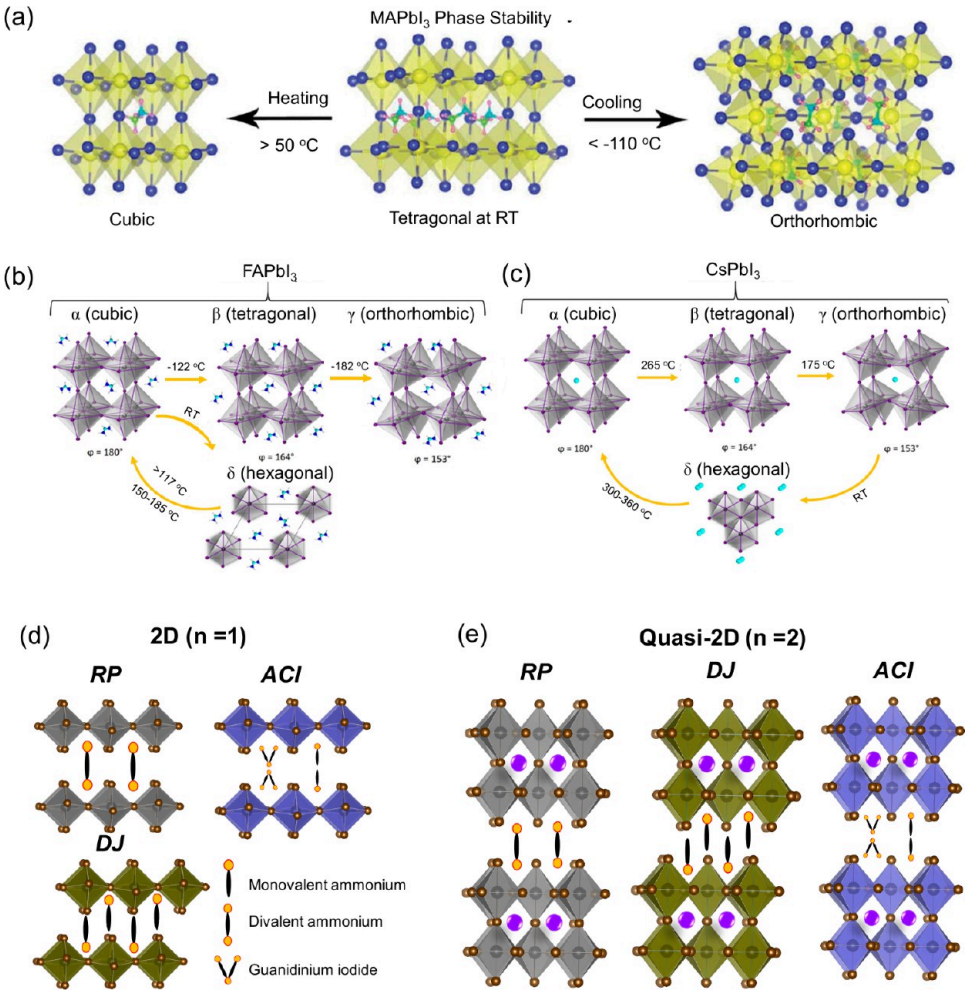

Figure 2. Crystal structure and temperature-dependent polymorphic phase transitions of (a) $MAPbI_3$, (b) $FAPbI_3$, and (c) $CsPbI_3$. Panel (a) has been reproduced with permission from ref 15. Copyright 2019, Royal Society of Chemistry, London. Panel (c) was reproduced with permission from ref 17. Copyright 2020, American Chemical Society, Washington, DC.] Representative crystal structures of Dion–Jacobson (DJ), Ruddlesden–Popper (RP), and alternative cations in the interlayer (ACI) in (d) pure 2D and (e) quasi-2D phases.

2. FUNDAMENTALS OF HALIDE PEROVSKITES

2.1. Structure of Halide Perovskite

PSCs have yet to reach their full potential, with the highest attainable PCE predicted by the Shockley–Queisser (SQ) limit being ~32% (Figure 1b).[11] The SQ limit provides a theoretical boundary for the maximum fraction of incident energy that can be converted into electrical energy for a single-junction solar cell, considering charge carrier recombination solely through radiative mechanisms. Therefore, effective management of charge carriers through device and material engineering is necessary to further improve the PCE value.

Typically, perovskite materials used in PSCs have a chemical formula of ABX_3, where A, B, and X represent monovalent organic or inorganic cations (such as methylammonium (MA: $CH_3NH_3^+$), formamidinium (FA: $HC(NH_2)_2^+$), cesium (Cs^+)), divalent metal cations (such as lead (Pb^{2+}), tin (Sn^{2+})), and monovalent halide anions (such as chloride (Cl^-), bromide (Br^-), and iodide (I^-)), respectively. These materials crystallize to form a unit cell, as depicted in Figure 1c, where B is present at the center of corner-sharing $(BX_6)^{4-}$ octahedra, while the A-site cation (coordinated to 12 X anions) resides within the cuboctahedral cavity formed between eight BX_6 octahedra network. This unique crystal structure allows the perovskite to accommodate various sizes of cations and anions, providing sufficient room for material engineering. In an ideal ABX_3 cubic perovskite structure, the lattice constant is described by the following equation:

$$a = 2(R_B + R_X) = \sqrt{2}(R_A + R_X) \quad (1)$$

where R_A, R_B, and R_X are the ionic radii of A, B, and X, respectively. The ratio of lattice constant equations gives Goldschmidt's tolerance factor (TF), which defines the geometric constraints to deduce possible crystal structure and its stability for any perovskite composition.

$$TF = \frac{R_A + R_X}{\sqrt{2}(R_B + R_X)} \quad (2)$$

For a stable 3D perovskite crystal structure, TF lies between 0.8 and 1 (Figure 1d).[12] The TF in the narrow range of (0.9–1) can form an ideal cubic structure, while lower TF values indicate a distorted perovskite structure, resulting in less symmetric tetragonal or orthorhombic crystal structures.[13] When TF exceeds 1, perovskite materials tend to form a hexagonal crystal structure with a change in the dimensionality from three-dimensional (3D) to two-dimensional (2D) or one-dimensional (1D).

https://doi.org/10.1021/accountsmr.4c00237
Acc. Mater. Res. 2024, 5, 1544–1557

The electronic band structure of the OIHP materials is primarily determined by the BX_6 building blocks through overlapping of the electronic orbitals of B and X sites (Figure 1e). The valence band maximum is formed by σ-antibonding orbital (Pb 6s−I 5p)*, while conduction band minimum comprises π-antibonding orbital (Pb 6p−I 5p)* and σ-antibonding orbital (Pb 6p−I 5p)*. The replacement of halide from I to Br or Br to Cl decreases the strength of spin−orbit coupling to increase bandgap value. Another factor influencing the bandgap is octahedral tilting, which alters the Pb−I−Pb angle. The A-site cation plays a critical role in the symmetry of perovskite lattice, or sometimes dynamic off-centering of B site cation due to lone pair electron, often results in distortion of perovskite octahedra. Therefore, even without directly participating in band structure formation, the shape, size, and charge distribution of the A-site cation can impact the resulting band structures. Figure 1f demonstrates that the absorbance range can be extended to the near-infrared region by simply replacing the A-site cation in the $APbI_3$ structure.[14]

2.2. Crystal Phases in Halide Perovskites

Usually, perovskite materials exhibit polymorphism, consisting of various phases under distinct temperature and fabrication conditions. The black photoactive phase of perovskite materials exists after their film fabrication; however, they transform to metastable phases during film storage or cell operation. The crystal properties of commonly used perovskites are discussed in this section.

$MAPbI_3$ was the pioneering perovskite material to be employed in solar cells, widely adopted for its low-temperature processability and suitable bandgap (1.55 eV). At room temperature (RT), $MAPbI_3$ adopts a tetragonal phase (I_4/mcm), characterized by the tilting of PbI_6 octahedra around the c-axis.[15] It undergoes a phase transition from tetragonal to the cubic phase ($Pm\bar{3}m$ space group) at the solar cell operational temperatures (Figure 2a).[16] Further phase transition to the orthorhombic phase ($Pnma$) occurs at a very low temperature of −110 °C, involving the tilting of PbI_6 octahedra out of the ab plane.

To address the phase transition of $MAPbI_3$ and further enhance PV performance, FA-based perovskites have been employed. Compared with $MAPbI_3$, $FAPbI_3$ offers exceptional optoelectronic properties, including a significantly longer carrier lifetime, because of the formation of large polarons facilitated by the faster reorientation of FA cations.[11] $FAPbI_3$ crystallizes into α-phase at a high temperature of 150−185 °C, providing higher thermal stability than $MAPbI_3$, thanks to the relatively larger and less-volatile FA cation. However, $FAPbI_3$ lacks structural stability at RT and tends to transform from photoactive cubic α-phase to nonperovskite yellow hexagonal δ-phase ($P6_3/mmc$) due to anisotropic strain in a preferential plane of its lattice at RT (Figure 2b). Other photoactive black phases, such as tetragonal β-phase ($P4/mbm$) and orthorhombic γ-phase ($P4/mbm$) exist at very low temperatures of −122 and −182 °C, respectively. These phase transitions occur due to the reduced energy for dynamic motion, which can break the symmetry of the cubic lattice through octahedral tilting and changes Pb−I−Pb tilting angle (ϕ).[17]

$CsPbI_3$ exhibits excellent thermal stability and a higher thermal-decomposition temperature, compared with its organic counterparts. The photoactive cubic black phase (α-$CsPbI_3$) is obtained at temperatures exceeding 300 °C.[17] It also exhibits other photoactive phases at lower temperature, due to a decreased tilting angle (ϕ) (see Figure 2c). Specifically, α-$CsPbI_3$ (ϕ = 180°) transforms to tetragonal β-$CsPbI_3$ (ϕ = 164°, $P4/mbm$) and orthorhombic γ-$CsPbI_3$ (ϕ = 153°, $Pbnm$) at 265 and 175 °C, respectively. $CsPbI_3$ exists in a nonperovskite yellow δ-phase ($Pnma$) at RT. These undesired phase transitions influence the electronic band structures and related optoelectronic properties.

The choice of A-site cations is quite limited in 3D perovskites due to the geometrical constraints imposed by the TF; however, layered 2D perovskites with bulky A-site cations offer significantly more flexibility and enhanced ambient stability due to hydrophobic bulky organic cations.[18] 2D perovskites are divided into three categories based on the structure of bulky organic cations (Figure 2d); Ruddlesden−Popper (RP), Dion−Jacobson (DJ), and alternating cations in the interlayer (ACI) space with chemical formula of $A_2'A_{n-1}B_nX_{3n+1}$ (A′ is monovalent), $A'A_{n-1}B_nX_{3n+1}$ (A′ is divalent), and $A'A_nB_nX_{3n+1}$ (A′ is guanidinium), respectively. Here, n represents the number of octahedral sheets present between organic spacer layers, which can be adjusted by tuning the perovskite precursor composition. In the case of RP perovskite, two layers of monovalent spacer cations (such as n-propylammonium, n-octylammonium, phenethylammonium, etc.) separate the inorganic octahedra sheets, where adjacent sheets display an in-plane displacement, offset by one octahedral unit (Figure 2d). Contrary to this, DJ perovskite is formed by a single layer of divalent spacer cations (such as 3-(aminomethyl) piperidinium, 1,4-butanediammonium, 1,3-propanediammonium, etc.) with no offset between adjacent inorganic sheets. These diammonium cations form hydrogen bonds at both ends with the inorganic octahedra, resulting in a highly stable structure. The ACI phase, reported to be formed exclusively by guanidinium cations, consist of two conventional A-site cations and one bulky A′ cation in the spacer layer.[19] Apart from pure 2D phases, when a small amount of bulky cation is added to the 3D perovskite precursor, a phase transition from the 3D phases (cubic, tetragonal, and orthorhombic) to the layered structure is observed. This configuration is described as quasi-2D ($1 \leq n \leq 5$) or quasi-3D ($n \geq 5$) or mixed 2D-3D perovskite, as presented in Figure 2e.

3. CHALLENGES AND METHODOLOGIES TO IMPROVE DEVICE STABILITY AND PERFORMANCE

The perovskite films are widely prepared by one- and two-step deposition methods. In the one-step method, perovskite film is formed by spin coating a single perovskite precursor, which is prepared by mixing PbI_2 and organic/inorganic halides in polar aprotic solvents (dimethyl sulfoxide (DMSO) and γ-butyrolactone (GBL), dimethylformamide (DMF)). Then wet films are annealed at a certain temperature (T >100 °C) to control the nucleation and growth process via solvent evaporation. Here, controlled crystallization is crucial to produce good quality perovskite films (uniform, pinhole-free, highly crystalline) that can be accomplished by forming stable intermediate through Lewis acid−base adduct or antisolvent dripping to extract the polar aprotic precursor solvents. In the two-step deposition, a perovskite film is formed by first spin coating a PbI_2 layer from Pb precursor (Pb halides in DMF) and annealing it at 70 °C for 1 min. Then perovskite film is formed through a thermal interdiffusion process by exposing the PbI_2 layer to organic salts through spin coating, dipping, or thermal evaporation. However, the solution processed fabrication of

https://doi.org/10.1021/accountsmr.4c00237
Acc. Mater. Res. 2024, 5, 1544−1557

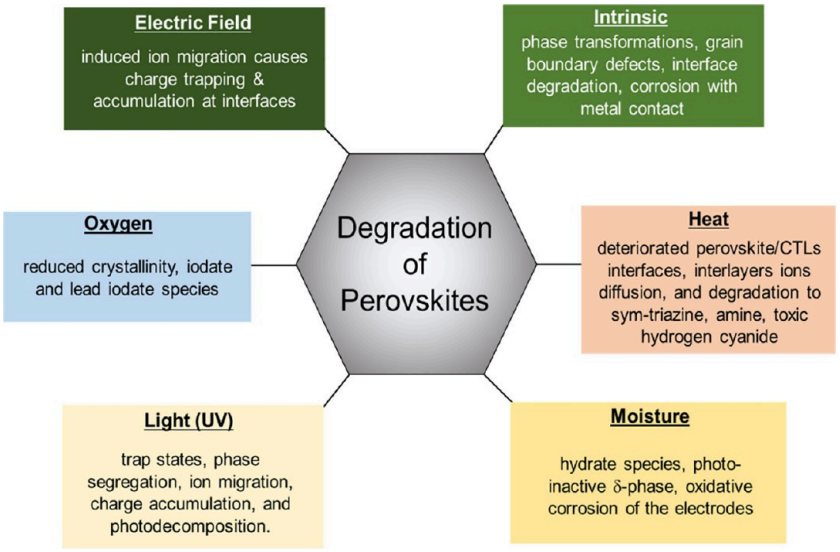

Figure 3. Intrinsic and extrinsic degradation mechanisms of PSCs under ambient and solar-cell working conditions.

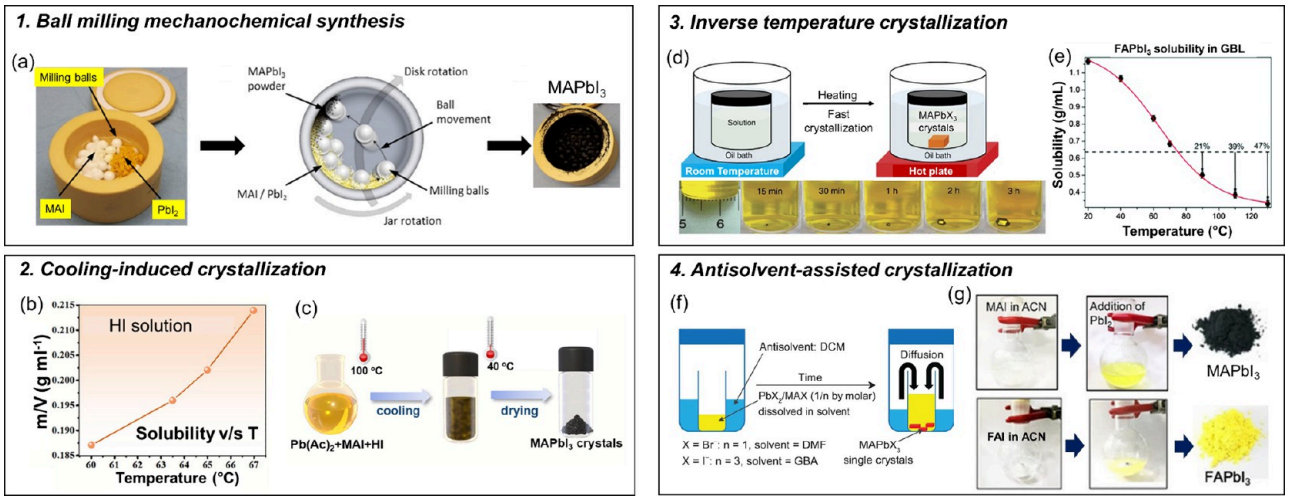

Figure 4. Single-crystal preparation methods. (a) Schematic representation and photograph of $MAPbI_3$ powder prepared by the ball milling method. [Reproduced with permission from ref 25. Copyright 2019, American Chemical Society, Washington, DC.] (b) Solubility curve of $MAPbI_3$ in HI solution and (c) single-crystal preparation via cooling-induced crystallization. [Reproduced with permission from ref 27. Copyright 2021, Elsevier.] (d) Schematics and photographs of precursor solution showing single-crystal formation by inverse-temperature crystallization method. [Reproduced with permission from ref 28. Copyright 2015, Springer Nature.] (e) Solubility curve of $FAPbI_3$ in GBL and photographs of obtained single crystals. [Reproduced with permission from ref 29. Copyright 2015, Royal Society of Chemistry, London.] (f) Graphic illustration of antisolvent-assisted crystallization. [Reproduced with permission from ref 30. Copyright 2015, AAAS.] (g) Photographs of $MAPbI_3$ and $FAPbI_3$ crystal powders prepared from low-grade PbI_2. [Reproduced with permission from ref 31. Copyright 2018, John Wiley and Sons.]

perovskite films is accompanied by various types of point defects and imperfections as discussed below.

3.1. Major Challenges and Strategies

Despite exhibiting impressive PV performance, the instability of PSCs remains a significant barrier to their commercial viability. Figure 3 illustrates the degradation of perovskites when exposed to moisture, heat, oxygen, electric fields, and prolonged light illumination, leading to chemical and structural instabilities along with loss of their light-harvesting properties.[20] Continuous illumination and thermal stress also affect the properties of HTLs, which often suffer from reduction of charge-transporting ability and migration of dopant from HTL to the bulk perovskite layer, reducing the performance and long-term stability.[21] The intrinsic degradation of PSC is triggered by surface defects, film inhomogeneity, ion migration, interlayer ions transfer, and corrosion with metal contact. The four main type of imperfections in PSCs include impurities (like Li^+ from doped HTL, Au/Ag from electrodes, contaminants from the raw materials), 2D extended defects (like grain boundaries and surface defects), and 3D defects like Pb clusters. These defects are responsible for ion migration and charge accumulation at interfaces, which imposes limitations on the performance and intrinsic stability of PSCs.[6] Therefore, various successful strategies, such as single crystal preparation, additive engineering, and interfacial passivation, are employed to tackle the above issues, as summarized in the sections below.

3.2. Single Crystal Growth

Fabrication of highly efficient PSCs using PbI_2 and organic/inorganic halides requires high-purity precursor materials (exceeding 99.999%), which increase their production cost

https://doi.org/10.1021/accountsmr.4c00237
Acc. Mater. Res. 2024, 5, 1544−1557

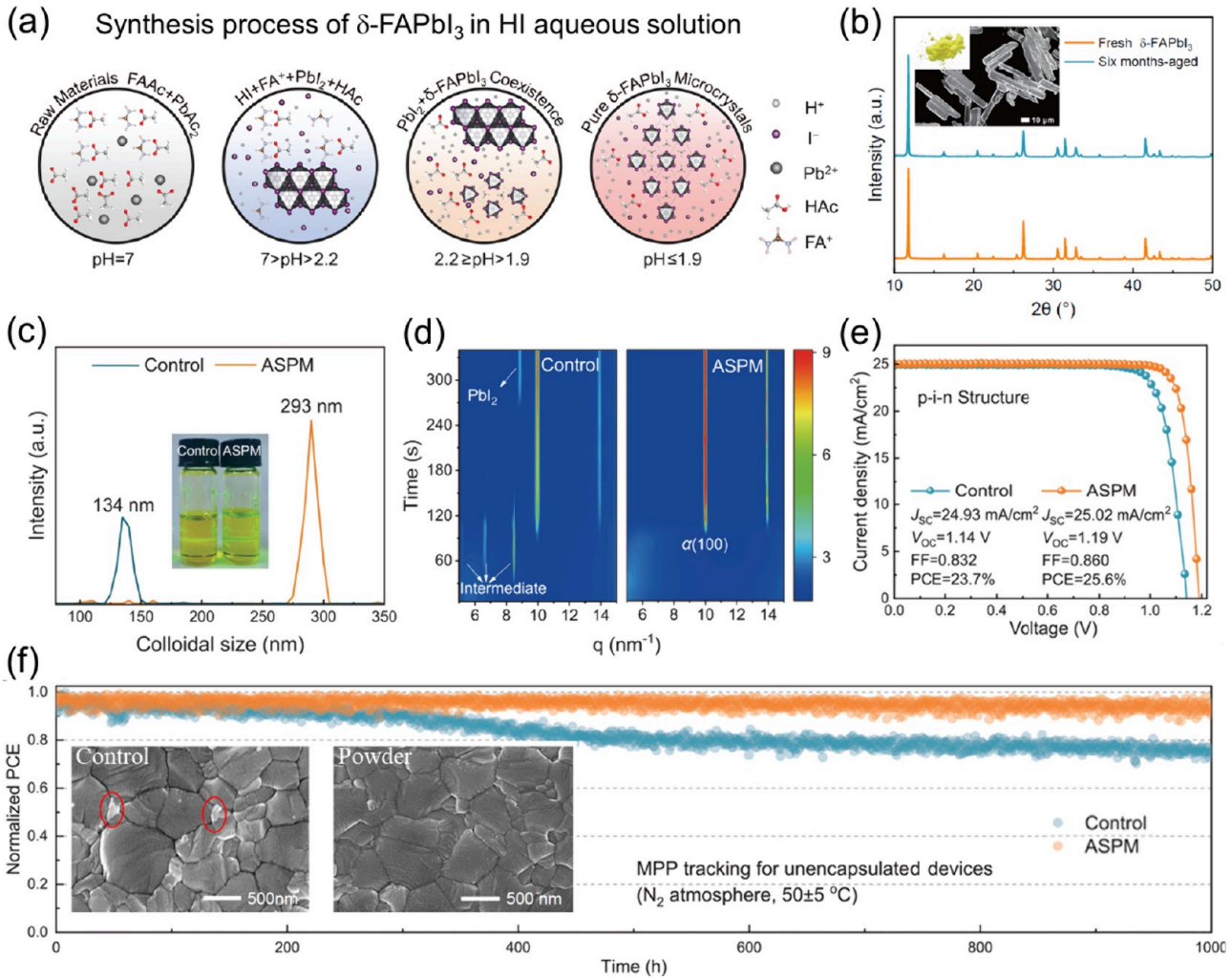

Figure 5. (a) Schematic illustration of $PbAc_2$ and FAAc at different pH values in HI aqueous solution, (b) XRD patterns of fresh and six-month aged δ-$FAPbI_3$ microcrystals, (c) dynamic light scattering, (d) in-situ GIWAXS measurements of the as-coated perovskite film, (e) *J*−*V* curves, and (f) PCE tracking at the MPP under continuous illumination for $FA_{0.85}MA_{0.1}Cs_{0.05}PbI_3$ prepared from the conventional mixture (control) and ASPM. [Reproduced with permission from ref 32. Copyright 2024, AAAS.]

and reduces batch-to-batch reproducibility, depending on the chemical supplier.[22] Moreover, mixing precursor materials on a microliter scale may lead to a nonstoichiometric perovskite with unreacted constituents, causing reduced performance.[23,24] Therefore, a cost-effective method that can produce high-efficiency PSCs by utilizing low-grade precursor materials is required for commercialization feasibility. One of the most effective approaches to achieve this goal is the synthesis of high-quality perovskite microcrystal powders to redissolve as precursors for perovskite film preparation in a low-cost and reproducible manner. Consequently, resultant perovskite films can inherit the exceptional characteristics of the parent perovskite crystals, such as high crystallinity, preferential crystal orientation, high purity, accurate stoichiometric ratio, low trap-state density, well-controlled phase distribution and structural arrangement, and good ambient and phase stability.

The strategies for preparation of perovskite single-crystal materials are divided into two categories: mechanochemistry (ball-milling) and wet chemistry (cooling-induced, inverse-temperature, and antisolvent-assisted crystallizations), as depicted in Figure 4. The low formation energy of the OIHP materials allows their synthesis via facile ball-milling of constituent salts (PbX_2 and AX) with the desired stoichiometry at RT (Figure 4a). This is a simple and efficient solvent-free method; however, the resultant product contains unreacted precursor impurities and nonuniform particles.[25] T-controlled crystallization can be used to prepare phase pure single crystals based on the type of precursor solvent by utilizing the retrograde solubility phenomenon. For example, in the case of halogen acids, the solubility of perovskite materials decreases with reduced temperature, whereas the solubility decreases with increases in temperature for DMF, DMSO, 2-methoxyethanol (2-ME), and γ-butyrolactone (GBL) solvents.[26] The drastic reduction in the solubility of $MAPbI_3$ in HI solution (Figure 4b) encouraged the use of cooling-induced crystallization method.[27] As shown in Figure 4c, cooling of a HI solution of lead acetate ($Pb(Ac)_2$) and MAI from 100 °C to 40 °C can lead to the formation of highly pure $MAPbI_3$ crystals. Here, controlling the cooling rate is important to modulate crystallization process, size, and shape of crystals.

Next, inverse-temperature crystallization utilizes the abnormal inverse T-induced solubility of perovskite materials in commonly used solvents (DMF, DMSO, 2-ME, and GBL). Figure 4d displays the photographs of $MAPbI_3$ single crystal formation by heating the saturated solution at 100 °C within 3 h.[28] Figure 4e shows the retrograde solubility curve of $FAPbI_3$

https://doi.org/10.1021/accountsmr.4c00237
Acc. Mater. Res. 2024, 5, 1544−1557

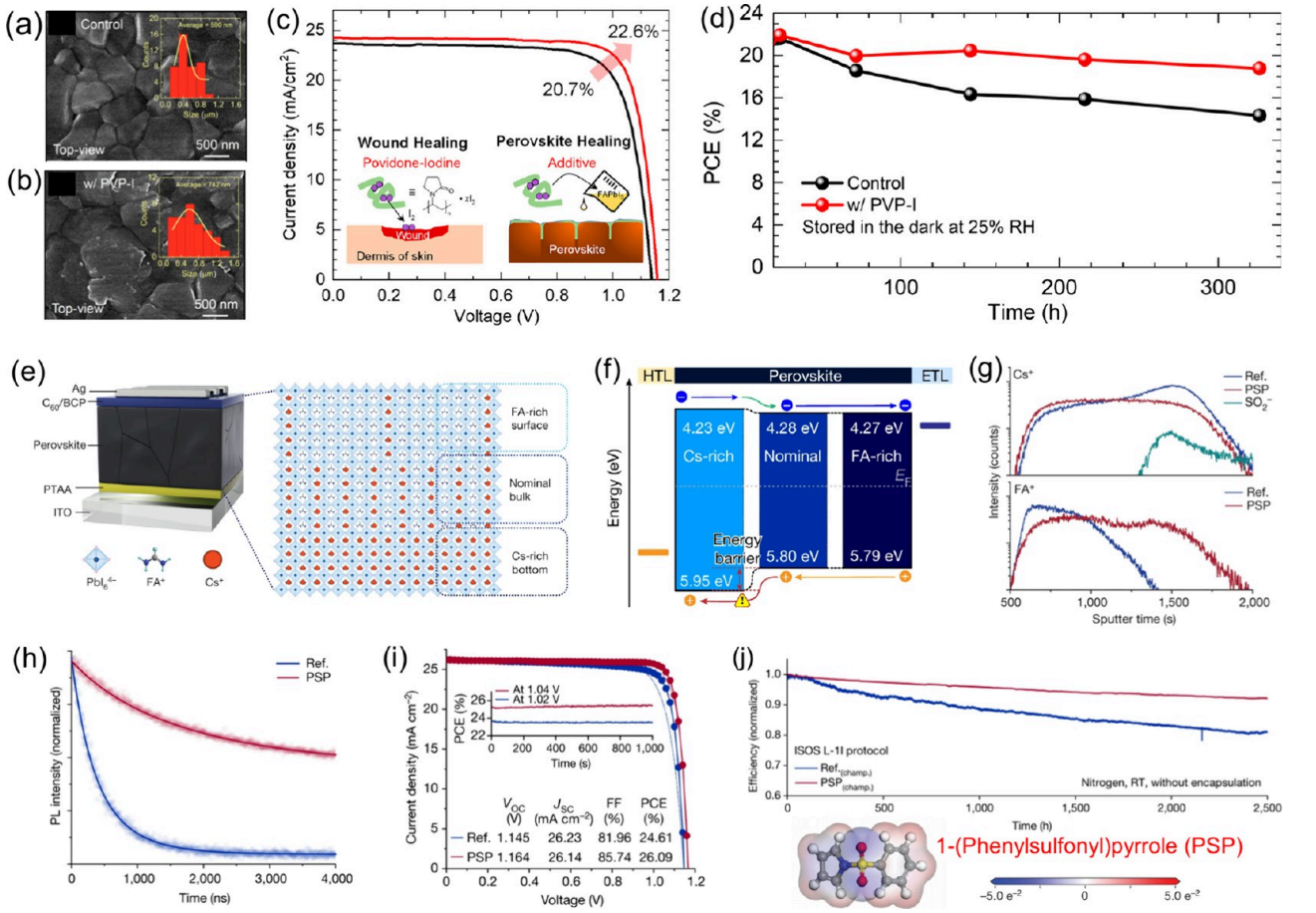

Figure 6. (a, b) Surface morphology, (c) J−V curve, and (d) stability under dark storage for control and PVP-I additive-based perovskites. [Reproduced with permission from ref 37. Copyright 2022, American Chemical Society, Washington, DC.] (e) Schematic illustration of out-of-plane cation inhomogeneity in $FA_{1-x}Cs_xPbI_3$ perovskites, (f) band alignment in the reference perovskite film, (g) cation distribution from time-of-flight secondary ion mass spectrometry, (h) TRPL spectra, (i) J−V curves, and (j) PCE tracking at MPPT for reference and PSP-treated perovskite films and devices. [Reproduced with permission from ref 38. Copyright 2023, Springer Nature.]

in GBL, where solubility is drastically reduced by heating the solution from 20 to 120 °C.[29] The fast crystallization rate in this method produces single crystals very quickly.

Figure 4f illustrates the antisolvent-assisted crystallization process, where perovskite precursor is sealed in a closed vessel along with antisolvent.[30] The high-quality $MAPbX_3$ single crystals are obtained by slow diffusion of the antisolvent vapors (dichloromethane) into a perovskite solution. Our group was among the pioneers to produce single crystal powders of $MAPbI_3$ and δ-$FAPbI_3$ by employing this method (Figure 4g).[31] An intriguing liquid−solid phase reaction was proposed where MAI dissolved in acetonitrile (ACN) produces MA and I ions. When low-grade PbI_2 was slowly added, it was dissolved with the assistance of I^- to form iodoplumbate $(PbI_2{\cdot}xI)^-$, then additional amount of PbI_2 reacts with MA and I^- ions to form a black-colored $MAPbI_3$ powder. PSCs prepared by using the synthesized powder displayed a relatively high PCE surpassing that for high-purity PbI_2, along with better reproducibility.

In a recent groundbreaking work, we reported the versatile aqueous synthesis for the production of ultrapure perovskite microcrystals, providing a low-cost route without the use of organic solvents.[32] In this work, kilogram-scale mass production of $FAPbI_3$ microcrystals with a purity of 99.996% was possible from inexpensive and low purity raw materials, resulting in a significant reduction in overall material costs. $FAPbI_3$ microcrystals were prepared using aqueous-soluble lead acetate trihydrate ($PbAc_2{\cdot}3H_2O$, 99.5%) and formamidine acetate (FAAc, 99%) in a HI aqueous solution (Figure 5a). The favorable pH of <1.9 was maintained for intercalation of FA ions into $PbI^{x-}{}_{(2+x)}$ scaffolds to produce $FAPbI_3$ crystals. The hexagonal δ-phase yellow powder with 1D rodlike morphology was obtained, which demonstrated excellent six-month stability under ambient storage (Figure 5b). The ternary-cation $FA_{0.85}MA_{0.1}Cs_{0.05}PbI_3$ perovskite precursor was prepared using mixture of $FAPbI_3$, $MAPbI_3$, and $CsPbI_3$ microcrystals for characterizing film and device, all obtained from the similar method (ASPM). Figure 5c shows the colloids sizes of 134 and 293 nm in control and ASPM-based precursors, respectively, which contribute to forming better-quality perovskite films. The control film shows the formation of α-$FAPbI_3$ through intermediate states and contains a PbI_2 peak, whereas the ASPM film formed directly from $FAPbI_3$ colloids without any parasitic phases and enhanced crystallinity (Figure 5d). Finally, the PCE of inverted (p-i-n) devices increased from 23.7% (control) to 25.6% for ASPM, because of the significantly lower trap states and improved charge-transport properties (Figure 5e). In terms of operational stability, PSCs based on ASPM kept 94% of the initial PCEs after 1000 h under continuous illumination (Figure 5f).

https://doi.org/10.1021/accountsmr.4c00237
Acc. Mater. Res. 2024, 5, 1544−1557

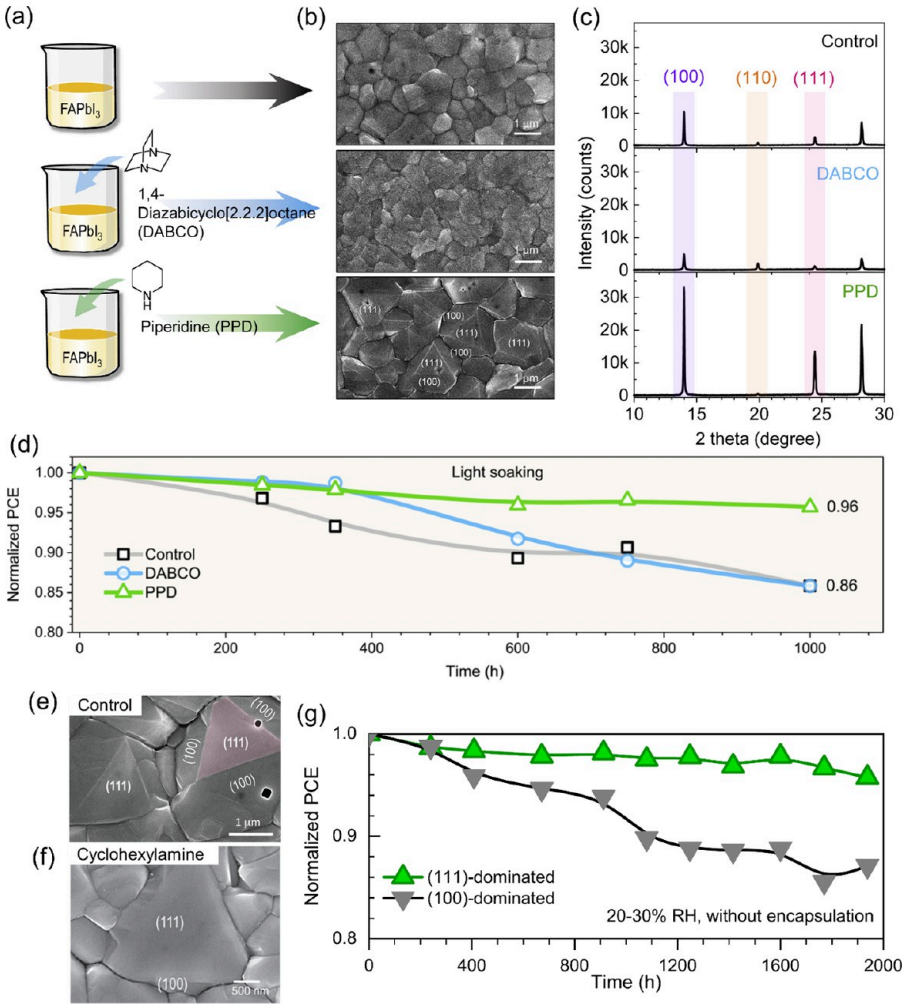

Figure 7. (a) Schematic representation of additive incorporation, (b) SEM images, (c) XRD patterns of perovskite films, and (d) light soaking stability of control and additive-based cells. Reproduced with permission from ref 39. Copyright 2022, Elsevier. SEM images of (e) control and (f) cyclohexylamine additive-based perovskite films. (g) Stability test for storage at RH = 30%−40% in air. [Reproduced with permission from ref 40. Copyright 2023, AAAS.]

3.3. Additive Engineering

The uncontrollable crystallization causes bulk and surface defects, resulting in the recombination of photogenerated charge carriers and degradation under external stress due to ion migration and charge carrier accumulation at interfaces.[33,34] Additive engineering has been employed to passivation bulk defects, improve perovskite film morphology, and regulate crystallization via coordination bonding with perovskite.[35] For example, phosphorus (P)-, nitrogen (N)-, sulfur (S)-, and oxygen (O)-containing Lewis base molecules were reported to form intermediate adducts for favorable crystallization and passivate undercoordinated Pb on grain boundary to decrease defect density, suppress ion migration, and enhance stability.[36] Our group used polyvinylpyrrolidone as an additive to mimic its healing properties via povidone−iodine (PVP-I) complex.[37] It acted as a reservoir of iodine and helped in grain-boundary healing, enlarging the grain size because of a positive effect on crystal growth kinetics (Figures 6a and 6b). PSCs prepared with PVP-I exhibited significantly improved PCE (20.7%−22.6%) and device stability by keeping 97.53% of initial PCE after 350 h of storage under dark conditions (Figures 6c and 6d).

Most of the high-efficiency PSCs are based on FA-rich perovskite compositions with some amount of small size cations such as Cs to stabilize the perovskite lattice ($FA_{1-x}Cs_xPbI_3$). However, they suffer from cation inhomogeneity as Cs prefer to aggregate at the bottom of perovskite film (Figure 6e), which has a negative impact on PV performance of PSCs, because of blocking the interfacial charge transport (Figure 6f).[38] This out-of-plane inhomogeneity may result from solubility difference of Cs and FA components or soft base property of Cs^+, compared to FA^+, which leads to stronger interaction with PbI_3^-, thus preferentially aggregates at the bottom. However, in this novel work, 1-(phenylsulfonyl)-pyrrole (PSP) was synthesized as an additive for homogeneous distribution of cations throughout the perovskite film (Figure 6g). Introduction of PSP additive was found to accelerate both crystallization and phase transition, thereby inhibiting the segregation of FA and Cs phases. The carrier lifetime was increased from 491.7 to 1876.6 ns due to the increased defects formation energy that lowered the trap densities (Figure 6h). Consequently, PSP-treated *p*−*i*−*n* structured device reached a maximum PCE of 26.1% (certified PCE of 25.8%) and showed exceptional device stability by retaining 92% of initial PCE after 2500 h of MPPT in N_2 atmosphere (Figures 6i and 6j).

https://doi.org/10.1021/accountsmr.4c00237
Acc. Mater. Res. 2024, 5, 1544−1557

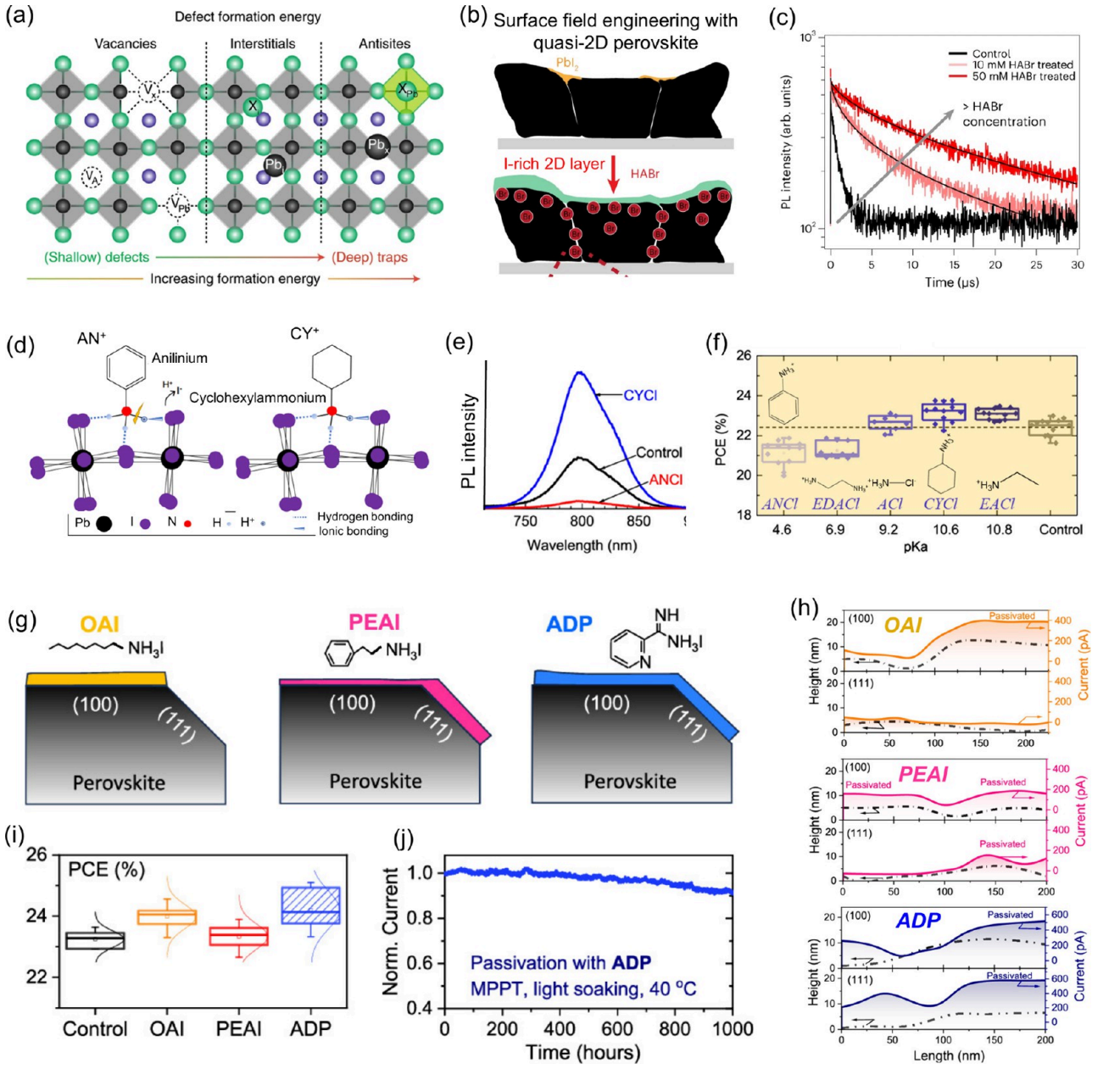

Figure 8. (a) Schematic representation of typical point defects in a perovskite crystal lattice based on their formation energy. [Reproduced with permission from ref 42. Copyright 2018, Springer Nature.] (b) Schematics of the working mechanism of HABr treatment on the perovskite surface and (c) TRPL decay curves of control and HABr-treated samples. [Reproduced with permission from ref 44. Copyright 2024, Springer Nature.] (d) Interaction of ammonium salts and perovskite octahedra, (e) steady-state PL, and (f) PCE comparison of various passivation materials with different pK_a values. [Reproduced with permission from ref 45. Copyright 2021, American Chemical Society, Washington, DC.] (g) Schematic representation, (h) current and height profiles, (i) PCE comparison of OAI, PEAI, and ADP-treated perovskites. and (j) light soaking stability of ADP-passivated device. [Reproduced with permission from ref 46. Copyright 2023, American Chemical Society, Washington, DC.]

It is highly desirable to produce perovskite thin films with single crystal-like grains, having well-defined facets that result in defect-free films and can approach theoretical PV limits without the need of passivation strategies. We reported the formation of well-defined facets on perovskite film by exquisite control of the film formation process and identified the facets with superior PV performance.[39] The well-defined (100) and (111) facets (triangular facet surrounded by lateral facets) were obtained for $FAPbI_3$ perovskite films prepared by piperidine (PPD) as an additive whereas 1,4-diazabicyclo[2.2.2]octane (DABCO)-additive-based films exhibited (110) facets (topographic stripes) (Figures 7a–c). PPD can strongly attach to the (100) and (111) facets to reduce their surface energies. The (100) and (111) facets showed high carrier mobility and low trap density compared to the (110) facet. The crystallization kinetics revealed the rapid formation of α-phase in the presence of PPD due to the low energy barrier for δ to α-phase transformation. The PPD-based PSC displayed higher PCE along with improved stability under continuous illumination (Figure 7d).

In another interesting work, the role of different crystal facets on stability and their underlying degradation mechanism was revealed.[40] It helped in developing a fundamental understanding about the overall stability of perovskite films

https://doi.org/10.1021/accountsmr.4c00237
Acc. Mater. Res. 2024, 5, 1544−1557

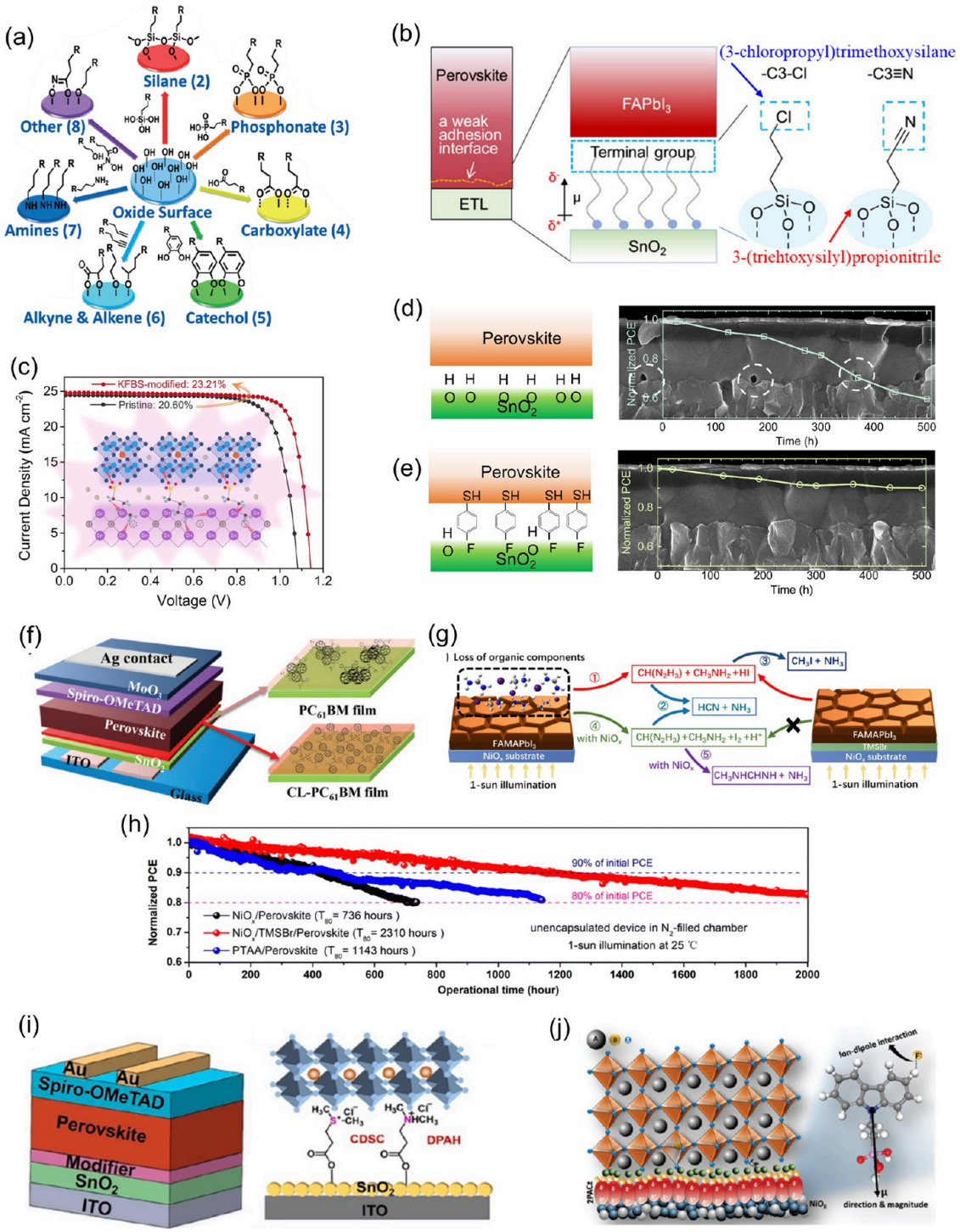

Figure 9. (a) Binding scheme of various organic materials on the oxide surface. [Reproduced with permission from ref 47. Copyright 2014, John Wiley and Sons.] (b) Schematics for buried interface passivation via siloxane-based self-assembled monolayer. [Reproduced with permission from ref 48. Copyright 2024, Elsevier.] (c) $J-V$ curve of control and KFBS-treated devices along with possible interaction among KFBS, SnO_2, and perovskite. [Reproduced with permission from ref 49. Copyright 2022, Elsevier.] Schematic surface structure of SnO_2 and cross-sectional SEM images along with long-term stability data (d) before and (e) after post-treatment of the SnO_2 surface by 4-fluorothiophenol (FT). [Reproduced with permission from ref 50. Copyright 2023, Royal Society of Chemistry, London.] (f) Device structure with different fullerene passivation agents at the buried interface. [Reproduced with permission from ref 51. Copyright 2023, John Wiley and Sons.] (g) Possible degradation mechanism of the $FAMAPbI_3$ at the NiO_x interface under illumination and (h) operational stability of the fabricated PSCs. [Reproduced with permission from ref 52. Copyright 2022, Royal Society of Chemistry, London.] (i) Device structure and depiction of interaction of CDSC or DPAH between SnO_2 and perovskite. [Reproduced with permission from ref 53. Copyright 2022, Elsevier.] (j) Schematic depiction of buried interface in the presence of ion dipole interaction between SAM with KF. [Reproduced with permission from ref 54. Copyright 2024, John Wiley and Sons.]

as the thermodynamically unstable facet can drive the perovskite degradation. It was noted that (100) facets are more susceptible to moisture-induced degradation than (111) facets, which motivated us to achieve a higher surface fraction

https://doi.org/10.1021/accountsmr.4c00237
Acc. Mater. Res. 2024, 5, 1544−1557

of (111) facets by employing cyclohexane (CHA)-additive (Figures 7e and 7f). The (111)-dominated device showed remarkable stability under humid conditions, maintaining 95% of the initial PCE after 2000 h (Figure 7g).

3.4. Device Architecture and Interface Engineering

The ambipolar charge transport behavior of the OIHP materials allows flexibility in designing various device architectures for PSCs. Typically, PSCs are fabricated in two architectures; normal ($n-i-p$) and inverted ($p-i-n$), classified based on the side facing the incident light or the type of CTLs deposited on transparent conducting oxides (FTO or ITO). The interfaces between the perovskite layer and the CTLs contain 100 times higher defect concentration than that of perovskite bulk, including deep-level defects (Figure 8a).[41,42] Therefore, passivation of both surface and buried interface by coordinate bonding, ionic bonding, or chemical conversion is required to improve energy level alignment, interfacial charge transport, mitigation of ion migration, and long-term stability of PSCs.[43]

Recently, a unique surface passivation strategy was reported, where surface treatment with hexylammonium bromide resulted in simultaneous formation of iodide-rich 2D layer on top of reference 3D perovskite film along with generation of bromide gradient extending from surface to bulk as shown in Figure 8b.[44] By optimization of the top interface, a record carrier lifetime of more than 30 μs was obtained (Figure 8c).

The surface passivation strategy has become eminent; however, the criteria for selecting suitable passivation materials are not well-defined. Therefore, this study from our group provided a good understanding about the selection of post-treatment materials based on the acid dissociation constant (pK_a) values.[45] For example, basicity of cyclohexylammonium (CYCl) is higher than anilinium chloride (ANCl) due to the inductive effect of the 6-membered C ring; therefore, it is a weaker conjugate acid (higher pK_a) due to stronger $N-H^+$ bond. So, ANCl can easily undergo deportation to release H^+ and mobile I^- ions, which increases the trap density and nonradiative recombinations (Figure 8d, e). The CYCl-treated PSC showed the highest PCE of 24.98%, compared to 21.07% (ANCl) (Figure 8f).

Furthermore, we reported a unique passivation approach based on selective anchoring of passivating agents with the facets of perovskite films as shown in Figure 8g.[46] We observed that the atomic arrangements of the facets determine the alignments and interactions of passivation materials. Based on a comparison between different passivation materials (phenethylammonium iodide (PEAI), octylammonium iodide (OAI), and 2-amidinopyridine hydroiodide (ADP)) with and without π electrons, it was found that six delocalized π electrons in the aromatic group can form adducts with (111) facets by donating electrons and also passivate (100) facets by their functional groups, while aliphatic materials like OAI can passivate only (100) facets. Therefore, it was proposed that (100) facets are sensitive to specific functional groups such as amines and acetic acids and to ions (ammonium and sulfide), whereas (111) facets are relatively insensitive and can interact with electron-rich phenyl groups or organic anions. The surface current density is increased after respective passivation as shown in Figure 8h. ADP-based PSCs showed the highest PCE of 25.10%, along with improved stability with just 10% degradation under MPPT for 1000 h, because of the effective passivation of both facets (Figures 8i and 8j).

Next, the effective buried interface passivation can be achieved by employing various types of organic functional molecules such as silane, phosphonate, carboxylate, amines, etc., as shown in Figure 9a.[47] Generally, a weak adhesion heterojunction is formed at the buried interface of CTLs/perovskite junction due to compositional inhomogeneity and strain in the perovskite layer. This poses a serious stability concern due to enhanced ion migration driven by a built-in electric field at this interface. Therefore, we focused our research on understanding interface-stability relation and employed silane derivates with self-assembled monolayer (SAM) characteristics at buried interface (Figure 9b). It favorably adjusted the energy level alignment to reduce built-in electric field and mitigate ion migration, thereby increasing the PCE up to 25.3% with stand-out stability by keeping 97% of initial PCE under MPPT after 1000 h.[48]

Wu et al. utilized synergistic effects of multifunctional potassium nonafluoro-1-butanesulfonate (KFBS) to favorably tune the energy level alignment at the perovskite/SnO_2 interface, enhance optoelectronic properties of both perovskite and ETL, and suppress interface and bulk defects. The treated devices displayed a significant increase in PCE from 20.6% to 23.21% (Figure 9c).[49] In yet another report from our group, the hydroxyl groups on the SnO_2 surface were effectively reduced by treating with 4-fluorothiophenol (FT), see Figure 9d, e. The reduction of pinholes at SnO_2/perovskite surface and increased device stability after 500 h of ambient storge underlines the effective passivation of hydroxyl defects which would otherwise induce deprotonation of MA^+.[50] Ding et al. reported that inserting a thin cross-linked PCBM layer for ion immobilization cab effectively eliminate the commonly observed burn-in degradation of PSCs (Figure 9f).[51] NiO_x-based p-i-n structured devices suffer from light-induced degradation due to multistep photochemical reactions shown in Figure 9g. Wu and co-workers addressed this issue by employing an aprotic trimethylsulfonium bromide-based buffer layer, which enabled exceptional photothermal stability, maintaining 82.8% of the initial PCE under continuous illumination for 2000 h (Figure 9h).[52] Another sulfonium-based material, 2-carboxyethyl dimethyl sulfonium chloride, act as a bridge between SnO_2 and perovskite layers to passivates interfacial defects via coordinate covalent bonding with both Sn^{2+} (SnO_2) and Pb^{2+} (perovskite) (Figure 9i).[53] Wang et al. reported an interesting strategy to increase the dipole moment of SAM through ion-dipole interaction by inserting a layer of ionic compounds (potassium and ammonium fluorides) between NiOx/SAM and the perovskite layer (Figure 9j). Consequently, increasing the work function of NiO_x for enhanced hole transport and device performance.[54]

4. SUMMARY AND PERSPECTIVE

We discuss the key fundamental properties crucial to high PV performance in PSCs. Next, we highlighted the key limiting factors, such as phase instability, recombination losses, ion migration, and interface and bulk defects, and described the degradation mechanism under various external stimuli, including moisture, ambient air, light, and heat. Based on these issues, we discussed various commonly reported device and precursor engineering approaches to mitigate the negative effects of these limiting factors. However, it can be concluded from the whole discussion that aqueous synthesis of perovskite microcrystals, additives to produce well-defined crystal facets in perovskite thin films, and their atomic arrangement-based

https://doi.org/10.1021/accountsmr.4c00237
Acc. Mater. Res. 2024, 5, 1544−1557

surface passivation hold the promise to drive this PV technology to meet the industrial standards by providing super high PCE and stability.

Furthermore, there are more tactical points that can be considered while moving this technology forward:

(1) Improving the intrinsic stability of PSCs by developing or stabilizing $FAPbI_3$ photoactive phases at RT and/or devising a whole new combination of perovskite composition by judicious choice of A/X sites with stable photoactive phases can eventually overcome perovskite instability under harsh conditions.
(2) Fabricating perovskite thin films with grains similar to single crystals having highly photoactive facets might result in defect-free thin films without the need of any passivation strategies. It can be brought to reality by manipulating the perovskite crystallization and growth process by target anchoring.
(3) The development of dopant-free charge transport materials also holds particular significance, as thermal and illumination stress during cell operation diffuse these dopants to different interlayers. At least robust interface materials are required that can block these ions diffusion processes without hindering the interfacial charge transport.

AUTHOR INFORMATION

Corresponding Author

Nam-Gyu Park − *School of Chemical Engineering and Center for Antibonding Regulated Crystals, Sungkyunkwan University, Suwon 16419, Republic of Korea; SKKU Institute of Energy Science and Technology (SIEST), Sungkyunkwan University, Suwon 16419, Republic of Korea;* orcid.org/0000-0003-2368-6300; Email: npark@skku.edu

Author

Sanjay Sandhu − *School of Chemical Engineering and Center for Antibonding Regulated Crystals, Sungkyunkwan University, Suwon 16419, Republic of Korea*

Complete contact information is available at: https://pubs.acs.org/10.1021/accountsmr.4c00237

Author Contributions

N.-G.P. and S.S. conceived the subject and S.S. wrote a draft. N.-G.P. edited the manuscript.

Notes

The authors declare no competing financial interest.

Biographies

Sanjay Sandhu is currently working as a postdoctoral researcher at School of Chemical Engineering, Sungkyunkwan University. He received his Ph.D. in Materials Science and Engineering from Dongguk University in 2024. He completed his B.S. and M.S. degrees in Physics Honors from Panjab University in 2015 and 2017, respectively. His research interests are primarily focused on material engineering of perovskites, metal oxides, and organic functional molecules for applications in solar cells, ambient light cells, and photodetectors.

Nam-Gyu Park is a Lifetime Distinguished Professor at the School of Chemical Engineering and Director of the SKKU Institute of Energy Science and Technology (SIEST), Sungkyunkwan University (SKKU). He received his B.S., M.S., and Ph.D. degrees from Seoul National University (SNU) in 1988, 1992, and 1995, respectively. He worked at ICMCB-CNRS, France, and National Renewable Energy Laboratory (NREL), USA, from 1996 to 1999 as a Postdoctoral Researcher. He worked as the Director of Solar Cell Research Center at the Korea Institute of Science and Technology (KIST) in Korea before joining SKKU as a Full Professor in 2009. He is the pioneer of the solid-state perovskite solar cell, discovered in 2012. He received the Clarivate Citation Laureates in Chemistry in 2017 and was consecutively selected as a Highly Cited Researcher since 2017.

ACKNOWLEDGMENTS

This work was supported by the National Research Foundation of Korea (NRF) grants funded by the Korean government (MSIT), under Contract Nos. NRF-2021R1A3B1076723 (Research Leader Program), NRF-2022M3J1A1085280 (Carbon Neutral Technology Program), and RS-2023-00259096 (GRDC Cooperative Hub).

REFERENCES

(1) Wang, S.; Wang, A.; Hao, F. Toward stable lead halide perovskite solar cells: A knob on the A/X sites components. *iScience* **2022**, *25* (1), 103599.
(2) Kim, H.-S.; Lee, C.-R.; Im, J.-H.; Lee, K.-B.; Moehl, T.; Marchioro, A.; Moon, S.-J.; Humphry-Baker, R.; Yum, J.-H.; Moser, J. E.; Grätzel, M.; Park, N.-G. Lead Iodide Perovskite Sensitized All-Solid-State Submicron Thin Film Mesoscopic Solar Cell with Efficiency Exceeding 9%. *Sci. Rep.* **2012**, *2* (1), 591.
(3) Zhou, J.; Tan, L.; Liu, Y.; Li, H.; Liu, X.; Li, M.; Wang, S.; Zhang, Y.; Jiang, C.; Hua, R.; Tress, W.; Meloni, S.; Yi, C. Highly efficient and stable perovskite solar cells via a multifunctional hole transporting material. *Joule* **2024**, *8*, 1691.
(4) Chen, H.; Liu, C.; Xu, J.; Maxwell, A.; Zhou, W.; Yang, Y.; Zhou, Q.; Bati, A. S. R.; Wan, H.; Wang, Z.; Zeng, L.; Wang, J.; Serles, P.; Liu, Y.; Teale, S.; Liu, Y.; Saidaminov, M. I.; Li, M.; Rolston, N.; Hoogland, S.; Filleter, T.; Kanatzidis, M. G.; Chen, B.; Ning, Z.; Sargent, E. H. Improved charge extraction in inverted perovskite solar cells with dual-site-binding ligands. *Science* **2024**, *384* (6692), 189−193.
(5) Khenkin, M. V.; Katz, E. A.; Abate, A.; Bardizza, G.; Berry, J. J.; Brabec, C.; Brunetti, F.; Bulović, V.; Burlingame, Q.; Di Carlo, A.; Cheacharoen, R.; Cheng, Y.-B.; Colsmann, A.; Cros, S.; Domanski, K.; Dusza, M.; Fell, C. J.; Forrest, S. R.; Galagan, Y.; Di Girolamo, D.; Grätzel, M.; Hagfeldt, A.; von Hauff, E.; Hoppe, H.; Kettle, J.; Köbler, H.; Leite, M. S.; Liu, S.; Loo, Y.-L.; Luther, J. M.; Ma, C.-Q.; Madsen, M.; Manceau, M.; Matheron, M.; McGehee, M.; Meitzner, R.; Nazeeruddin, M. K.; Nogueira, A. F.; Odabaşı, Ç.; Osherov, A.; Park, N.-G.; Reese, M. O.; De Rossi, F.; Saliba, M.; Schubert, U. S.; Snaith, H. J.; Stranks, S. D.; Tress, W.; Troshin, P. A.; Turkovic, V.; Veenstra, S.; Visoly-Fisher, I.; Walsh, A.; Watson, T.; Xie, H.; Yıldırım, R.; Zakeeruddin, S. M.; Zhu, K.; Lira-Cantu, M. Consensus statement for stability assessment and reporting for perovskite photovoltaics based on ISOS procedures. *Nat. Energy* **2020**, *5* (1), 35−49.
(6) Li, X.; Yang, H.; Liu, A.; Lu, C.; Yuan, H.; Zhang, W.; Fang, J. Iodine-trapping strategy for light-heat stable inverted perovskite solar cells under ISOS protocols. *Energy Environ. Sci.* **2023**, *16* (12), 6071−6077.
(7) Suo, J.; Yang, B.; Mosconi, E.; Bogachuk, D.; Doherty, T. A. S.; Frohna, K.; Kubicki, D. J.; Fu, F.; Kim, Y.; Er-Raji, O.; Zhang, T.; Baldinelli, L.; Wagner, L.; Tiwari, A. N.; Gao, F.; Hinsch, A.; Stranks, S. D.; De Angelis, F.; Hagfeldt, A. Multifunctional sulfonium-based treatment for perovskite solar cells with less than 1% efficiency loss over 4,500-h operational stability tests. *Nat. Energy* **2024**, *9* (2), 172−183.
(8) Zhou, S.; Fu, S.; Wang, C.; Meng, W.; Zhou, J.; Zou, Y.; Lin, Q.; Huang, L.; Zhang, W.; Zeng, G.; Pu, D.; Guan, H.; Wang, C.; Dong, K.; Cui, H.; Wang, S.; Wang, T.; Fang, G.; Ke, W. Aspartate all-in-one

doping strategy enables efficient all-perovskite tandems. *Nature* **2023**, *624* (7990), 69−73.
(9) Dai, Z.; You, S.; Chakraborty, D.; Li, S.; Zhang, Y.; Ranka, A.; Barlow, S.; Berry, J. J.; Marder, S. R.; Guo, P.; Qi, Y.; Zhu, K.; Padture, N. P. Connecting Interfacial Mechanical Adhesion, Efficiency, and Operational Stability in High Performance Inverted Perovskite Solar Cells. *ACS Energy Lett.* **2024**, *9* (4), 1880−1887.
(10) Shin, G. S.; Zhang, Y.; Park, N. G. Stability of Precursor Solution for Perovskite Solar Cell: Mixture (FAI + PbI_2) versus Synthetic $FAPbI_3$ Crystal. *ACS Appl. Mater. Interfaces* **2020**, *12* (13), 15167−15174.
(11) Liu, X.; Luo, D.; Lu, Z. H.; Yun, J. S.; Saliba, M.; Seok, S. I.; Zhang, W. Stabilization of photoactive phases for perovskite photovoltaics. *Nat. Rev. Chem.* **2023**, *7* (7), 462−479.
(12) Correa-Baena, J.-P.; Saliba, M.; Buonassisi, T.; Grätzel, M.; Abate, A.; Tress, W.; Hagfeldt, A. Promises and challenges of perovskite solar cells. *Science* **2017**, *358* (6364), 739−744.
(13) Wang, Z.; Shi, Z.; Li, T.; Chen, Y.; Huang, W. Stability of Perovskite Solar Cells: A Prospective on the Substitution of the A Cation and X Anion. *Angew. Chem., Int. Ed.* **2017**, *56* (5), 1190−1212.
(14) Eperon, G. E.; Stranks, S. D.; Menelaou, C.; Johnston, M. B.; Herz, L. M.; Snaith, H. J. Formamidinium lead trihalide: A broadly tunable perovskite for efficient planar heterojunction solar cells. *Energy Environ. Sci.* **2014**, *7* (3), 982−988.
(15) Arabpour Roghabadi, F.; Alidaei, M.; Mousavi, S. M.; Ashjari, T.; Tehrani, A. S.; Ahmadi, V.; Sadrameli, S. M. Stability progress of perovskite solar cells dependent on the crystalline structure: From 3D ABX3 to 2D Ruddlesden-Popper perovskite absorbers. *J. Mater. Chem. A* **2019**, *7* (11), 5898−5933.
(16) Conings, B.; Drijkoningen, J.; Gauquelin, N.; Babayigit, A.; D'Haen, J.; D'Olieslaeger, L.; Ethirajan, A.; Verbeeck, J.; Manca, J.; Mosconi, E.; Angelis, F. D.; Boyen, H.-G. Intrinsic Thermal Instability of Methylammonium Lead Trihalide Perovskite. *Adv. Energy Mater.* **2015**, *5* (15), 1500477.
(17) Masi, S.; Gualdrón-Reyes, A. F.; Mora-Seró, I. Stabilization of Black Perovskite Phase in $FAPbI_3$ and $CsPbI_3$. *ACS Energy Lett.* **2020**, *5* (6), 1974−1985.
(18) Mahmud, M. A.; Duong, T.; Peng, J.; Wu, Y.; Shen, H.; Walter, D.; Nguyen, H. T.; Mozaffari, N.; Tabi, G. D.; Catchpole, K. R.; Weber, K. J.; White, T. P. Origin of Efficiency and Stability Enhancement in High-Performing Mixed Dimensional 2D-3D Perovskite Solar Cells: A Review. *Adv. Funct. Mater.* **2022**, *32* (3), DOI: 10.1002/adfm.202009164.
(19) Zhang, Y.; Park, N.-G. Quasi-Two-Dimensional Perovskite Solar Cells with Efficiency Exceeding 22%. *ACS Energy Lett.* **2022**, *7* (2), 757−765.
(20) Wang, Z.; Shi, Z.; Li, T.; Chen, Y.; Huang, W. Stability of Perovskite Solar Cells: A Prospective on the Substitution of the A Cation and X Anion. *Angew. Chem., Int. Ed.* **2017**, *56* (5), 1190−1212.
(21) Kim, Y.; Kim, G.; Park, E. Y.; Moon, C. S.; Lee, S. J.; Yoo, J. J.; Nam, S.; Im, J.; Shin, S. S.; Jeon, N. J.; Seo, J. Alkylammonium bis(trifluoromethylsulfonyl)imide as a dopant in the hole-transporting layer for efficient and stable perovskite solar cells. *Energy Environ. Sci.* **2023**, *16* (5), 2226−2238.
(22) Chang, J.; Zhu, H.; Li, B.; Isikgor, F. H.; Hao, Y.; Xu, Q.; Ouyang, J. Boosting the performance of planar heterojunction perovskite solar cell by controlling the precursor purity of perovskite materials. *J. Mater. Chem. A* **2016**, *4* (3), 887−893.
(23) Shin, G. S.; Zhang, Y.; Park, N.-G. Stability of Precursor Solution for Perovskite Solar Cell: Mixture (FAI + PbI2) versus Synthetic FAPbI3 Crystal. *ACS Appl. Mater. Interfaces* **2020**, *12* (13), 15167−15174.
(24) Kerner, R. A.; Christensen, E. D.; Harvey, S. P.; Messinger, J.; Habisreutinger, S. N.; Zhang, F.; Eperon, G. E.; Schelhas, L. T.; Zhu, K.; Berry, J. J.; Moore, D. T. Analytical Evaluation of Lead Iodide Precursor Impurities Affecting Halide Perovskite Device Performance. *ACS Appl. Energy Mater.* **2023**, *6* (1), 295−301.
(25) Leupold, N.; Schötz, K.; Cacovich, S.; Bauer, I.; Schultz, M.; Daubinger, M.; Kaiser, L.; Rebai, A.; Rousset, J.; Köhler, A.; Schulz, P.; Moos, R.; Panzer, F. High Versatility and Stability of Mechanochemically Synthesized Halide Perovskite Powders for Optoelectronic Devices. *ACS Appl. Mater. Interfaces* **2019**, *11* (33), 30259−30268.
(26) Stoumpos, C. C.; Malliakas, C. D.; Kanatzidis, M. G. Semiconducting Tin and Lead Iodide Perovskites with Organic Cations: Phase Transitions, High Mobilities, and Near-Infrared Photoluminescent Properties. *Inorg. Chem.* **2013**, *52* (15), 9019−9038.
(27) Feng, W.; Liao, J.-F.; Chang, X.; Zhong, J.-X.; Yang, M.; Tian, T.; Tan, Y.; Zhao, L.; Zhang, C.; Lei, B.-X.; Wang, L.; Huang, J.; Wu, W.-Q. Perovskite crystals redissolution strategy for affordable, reproducible, efficient and stable perovskite photovoltaics. *Mater. Today* **2021**, *50*, 199−223.
(28) Saidaminov, M. I.; Abdelhady, A. L.; Murali, B.; Alarousu, E.; Burlakov, V. M.; Peng, W.; Dursun, I.; Wang, L.; He, Y.; Maculan, G.; Goriely, A.; Wu, T.; Mohammed, O. F.; Bakr, O. M. High-quality bulk hybrid perovskite single crystals within minutes by inverse temperature crystallization. *Nat. Commun.* **2015**, *6* (1), 7586.
(29) Saidaminov, M. I.; Abdelhady, A. L.; Maculan, G.; Bakr, O. M. Retrograde solubility of formamidinium and methylammonium lead halide perovskites enabling rapid single crystal growth. *Chem. Commun.* **2015**, *51* (100), 17658−17661.
(30) Shi, D.; Adinolfi, V.; Comin, R.; Yuan, M.; Alarousu, E.; Buin, A.; Chen, Y.; Hoogland, S.; Rothenberger, A.; Katsiev, K.; Losovyj, Y.; Zhang, X.; Dowben, P. A.; Mohammed, O. F.; Sargent, E. H.; Bakr, O. M. Low trap-state density and long carrier diffusion in organolead trihalide perovskite single crystals. *Science* **2015**, *347* (6221), 519−522.
(31) Zhang, Y.; Kim, S.-G.; Lee, D.-K.; Park, N.-G. $CH_3NH_3PbI_3$ and $HC(NH_2)_2PbI_3$ Powders Synthesized from Low-Grade PbI_2: Single Precursor for High-Efficiency Perovskite Solar Cells. *ChemSusChem* **2018**, *11* (11), 1813−1823.
(32) Zhu, P.; Wang, D.; Zhang, Y.; Liang, Z.; Li, J.; Zeng, J.; Zhang, J.; Xu, Y.; Wu, S.; Liu, Z.; Zhou, X.; Hu, B.; He, F.; Zhang, L.; Pan, X.; Wang, X.; Park, N.-G.; Xu, B. Aqueous synthesis of perovskite precursors for highly efficient perovskite solar cells. *Science* **2024**, *383* (6682), 524−531.
(33) Domanski, K.; Roose, B.; Matsui, T.; Saliba, M.; Turren-Cruz, S.-H.; Correa-Baena, J.-P.; Carmona, C. R.; Richardson, G.; Foster, J. M.; De Angelis, F.; Ball, J. M.; Petrozza, A.; Mine, N.; Nazeeruddin, M. K.; Tress, W.; Grätzel, M.; Steiner, U.; Hagfeldt, A.; Abate, A. Migration of cations induces reversible performance losses over day/night cycling in perovskite solar cells. *Energy Environ. Sci.* **2017**, *10* (2), 604−613.
(34) Duong, T.; Mulmudi, H. K.; Wu, Y.; Fu, X.; Shen, H.; Peng, J.; Wu, N.; Nguyen, H. T.; Macdonald, D.; Lockrey, M.; White, T. P.; Weber, K.; Catchpole, K. Light and Electrically Induced Phase Segregation and Its Impact on the Stability of Quadruple Cation High Bandgap Perovskite Solar Cells. *ACS Appl. Mater. Interfaces* **2017**, *9* (32), 26859−26866.
(35) Li, T.; Pan, Y.; Wang, Z.; Xia, Y.; Chen, Y.; Huang, W. Additive engineering for highly efficient organic-inorganic halide perovskite solar cells: recent advances and perspectives. *J. Mater. Chem. A* **2017**, *5* (25), 12602−12652.
(36) Yang, Z.; Dou, J.; Kou, S.; Dang, J.; Ji, Y.; Yang, G.; Wu, W.-Q.; Kuang, D.-B.; Wang, M. Multifunctional Phosphorus-Containing Lewis Acid and Base Passivation Enabling Efficient and Moisture-Stable Perovskite Solar Cells. *Adv. Funct. Mater.* **2020**, *30* (15), 1910710.
(37) Kang, D. H.; Ma, C.; Park, N. G. Antiseptic Povidone-Iodine Heals the Grain Boundary of Perovskite Solar Cells. *ACS Appl. Mater. Interfaces* **2022**, *14* (7), 8984−8991.
(38) Liang, Z.; Zhang, Y.; Xu, H.; Chen, W.; Liu, B.; Zhang, J.; Zhang, H.; Wang, Z.; Kang, D. H.; Zeng, J.; Gao, X.; Wang, Q.; Hu, H.; Zhou, H.; Cai, X.; Tian, X.; Reiss, P.; Xu, B.; Kirchartz, T.; Xiao, Z.; Dai, S.; Park, N. G.; Ye, J.; Pan, X. Homogenizing out-of-plane cation composition in perovskite solar cells. *Nature* **2023**, *624* (7992), 557−563.

(39) Ma, C.; Kang, M.-C.; Lee, S.-H.; Kwon, S. J.; Cha, H.-W.; Yang, C.-W.; Park, N.-G. Photovoltaically top-performing perovskite crystal facets. *Joule* **2022**, *6* (11), 2626−2643.
(40) Ma, C.; Eickemeyer, F. T.; Lee, S.-H.; Kang, D.-H.; Kwon, S. J.; Grätzel, M.; Park, N.-G. Unveiling facet-dependent degradation and facet engineering for stable perovskite solar cells. *Science* **2023**, *379* (6628), 173−178.
(41) Min, H.; Lee, D. Y.; Kim, J.; Kim, G.; Lee, K. S.; Kim, J.; Paik, M. J.; Kim, Y. K.; Kim, K. S.; Kim, M. G.; Shin, T. J.; Il Seok, S. Perovskite solar cells with atomically coherent interlayers on SnO_2 electrodes. *Nature* **2021**, *598* (7881), 444−450.
(42) Akkerman, Q. A.; Rainò, G.; Kovalenko, M. V.; Manna, L. Genesis, challenges and opportunities for colloidal lead halide perovskite nanocrystals. *Nat. Mater.* **2018**, *17* (5), 394−405.
(43) Chen, B.; Rudd, P. N.; Yang, S.; Yuan, Y.; Huang, J. Imperfections and their passivation in halide perovskite solar cells. *Chem. Soc. Rev.* **2019**, *48* (14), 3842−3867.
(44) deQuilettes, D. W.; Yoo, J. J.; Brenes, R.; Kosasih, F. U.; Laitz, M.; Dou, B. D.; Graham, D. J.; Ho, K.; Shi, Y.; Shin, S. S.; Ducati, C.; Bawendi, M. G.; Bulović, V. Reduced recombination via tunable surface fields in perovskite thin films. *Nat. Energy* **2024**, *9* (4), 457−466.
(45) Lee, S.-H.; Jeong, S.; Seo, S.; Shin, H.; Ma, C.; Park, N.-G. Acid Dissociation Constant: A Criterion for Selecting Passivation Agents in Perovskite Solar Cells. *ACS Energy Lett.* **2021**, 1612−1621.
(46) Ma, C.; Kang, M. C.; Lee, S. H.; Zhang, Y.; Kang, D. H.; Yang, W.; Zhao, P.; Kim, S. W.; Kwon, S. J.; Yang, C. W.; Yang, Y.; Park, N. G. Facet-Dependent Passivation for Efficient Perovskite Solar Cells. *J. Am. Chem. Soc.* **2023**, *145* (44), 24349−24357.
(47) Pujari, S. P.; Scheres, L.; Marcelis, A. T. M.; Zuilhof, H. Covalent Surface Modification of Oxide Surfaces. *Angew. Chem., Int. Ed.* **2014**, *53* (25), 6322−6356.
(48) Zhang, C.; Son, Y.; Kim, H.; Lee, S.-H.; Liang, X.; Fu, G.; Lee, S.-U.; Park, D.-A.; Jiang, Q.; Zhu, K.; Park, N.-G. Work function tuning of a weak adhesion homojunction for stable perovskite solar cells. *Joule* **2024**, *8* (5), 1394−1411.
(49) Wu, Z.; Wu, J.; Wang, S.; Wang, C.; Du, Y.; Wang, Y.; Geng, J.; Lin, Y.; Sun, W.; Lan, Z. Multifunctional molecule of potassium nonafluoro-1-butanesulfonate for high-efficient perovskite solar cells. *Chem. Eng. J.* **2022**, *449*, 137851.
(50) Jeon, Y.-S.; Kang, D.-H.; Kim, J.-H.; Park, N.-G. Stability and efficiency improvement of perovskite solar cells by surface hydroxyl defect passivation of SnO2 layer with 4-fluorothiophenol. *J. Mater. Chem. A* **2023**, *11* (7), 3673−3681.
(51) Ding, C.; Yin, L.; Wang, J.; Larini, V.; Zhang, L.; Huang, R.; Nyman, M.; Zhao, L.; Zhao, C.; Li, W.; Luo, Q.; Shen, Y.; Osterbacka, R.; Grancini, G.; Ma, C. Q. Boosting Perovskite Solar Cells Efficiency and Stability: Interfacial Passivation of Crosslinked Fullerene Eliminates the ″Burn-in″ Decay. *Adv. Mater.* **2023**, *35* (2), No. e2207656.
(52) Wu, T.; Ono, L. K.; Yoshioka, R.; Ding, C.; Zhang, C.; Mariotti, S.; Zhang, J.; Mitrofanov, K.; Liu, X.; Segawa, H.; Kabe, R.; Han, L.; Qi, Y. Elimination of light-induced degradation at the nickel oxide-perovskite heterojunction by aprotic sulfonium layers towards long-term operationally stable inverted perovskite solar cells. *Energy Environ. Sci.* **2022**, *15* (11), 4612−4624.
(53) Zuo, X.; Kim, B.; Liu, B.; He, D.; Bai, L.; Wang, W.; Xu, C.; Song, Q.; Jia, C.; Zang, Z.; Lee, D.; Li, X.; Chen, J. Passivating buried interface via self-assembled novel sulfonium salt toward stable and efficient perovskite solar cells. *Chem. Eng. J.* **2022**, *431*, 133209.
(54) Wang, S.; Khan, D.; Zhou, W.; Sui, Y.; Zhang, T.; Yu, G.; Huang, Y.; Yang, X.; Chen, X.; Yan, H.; Tang, J.; Yang, F.; Han, P.; Zheng, Z.; Zhang, Y.; Tang, Z. Ion-Dipole Interaction for Self-Assembled Monolayers: A New Strategy for Buried Interface in Inverted Perovskite Solar Cells. *Adv. Funct. Mater.* **2024**, DOI: 10.1002/adfm.202316202.

https://doi.org/10.1021/accountsmr.4c00237
Acc. Mater. Res. 2024, 5, 1544−1557